Journal of Applied Fluid Mechanics, Vol. 18, No. 2, pp. 317-331, 2025.
Available online at www.jafmonline.net, ISSN 1735-3572, EISSN 1735-3645.
https://doi.org/10.47176/jafm.18.2.2964

Pressure Drop Due to Cyclone Separator in Positive Dilute Phase Pneumatic Teff Grain Conveyor

L. D. Boset[1†], Z. A. Debele[2] and A. W. Koroso[1]

[1] *Adama Science and Technology University 1, Adama, Oromia, 0000, Ethiopia*
[2] *Faculty of Agriculture, University of Eswatini 2, Luyengo, Eswatini, M205, Eswatini*

†*Corresponding Author Email:lemi.demissie@astu.edu.et*

ABSTRACT

Cyclone separators are commonly used in pneumatic conveyor systems due to their low cost and ability to separate solid particles from gas streams. Understanding pressure drop in cyclone separators is crucial for designing, developing, and optimizing efficient cyclone separators for pneumatic conveyors. The swirling motion within the cyclone during particle-gas separation can cause a pressure drop in the pneumatic conveyor. This study investigates the pressure drop across cyclone separators in pneumatic conveyor systems for Teff grain, both experimentally and computational fluid dynamics (CFD) with discrete particle modeling (DPM) simulation. The study utilized the Lapple cyclone separator model and examined the effects of varying cyclone size (0.75D, 0.9D, and 1D for D=200mm), inlet air velocity (10m/s, 14m/s, 18m/s, 22m/s), and material mass flow rate (0.009kg/s, 0.03kg/s, 0.044kg/s, 0.067kg/s) on the pressure drop across the cyclone separator. The results show that there is strong agreement between experimental and CFD-DPM simulation results. The simulation results accurately represent experimental results, with R-squared value of 0.99 and a residual sum of squares of 38.018. Furthermore, the best curve fit was obtained between the power losses due to pressure drop across the cyclone separator and air mass flow rate. These findings demonstrate that the pressure drop and associated power losses across cyclone separators in pneumatic Teff grain conveyors can be effectively determined using both experimental and simulation methods. This finding can inform the design and optimization of efficient cyclone separators for pneumatic Teff grain conveyor systems.

Article History

Received July 7, 2024
Revised August 15, 2024
Accepted September 15, 2024
Available online December 4, 2024

Keywords:

Cyclone separator
Pressure drop
Pneumatic conveyor
Modeling
Teff grain

1. INTRODUCTION

Teff is the smallest grain in the world; it is a round, tiny, and difficult to handle without losing due to its size. (Zewdu, 2007; Ripp et al., 2015; Dula, 2016) a Teff grain is about 1/150 the size of a wheat kernel. The grain length ranges from 1.30 to 0.51 mm, and the grain width ranges from 0.67 to 0.10 mm, with a mean of 1.17 (0.59) to 0.61 (0.13) mm. Vandercasteelen et al. (2014) It is an important cereal crop indigenous to Ethiopia, where numerous form of diversity are also found. A gluten-free grain with highly regarded nutritional benefits has recently been attracting the attention of the modern food business. However, there isn't adequate information available on its handling and processing characteristics because it's a relatively new raw material for the modern industry Gonite (2018) in Ethiopia, Teff production, handling, and processing practices are dominated by traditional methods, and it is only mechanized to some extent, not as intensively as other cereal grains, because its nature is a major factor that challenges mechanization. Traditionally, the process of threshing Teff is time-consuming, laborious, and frequently requires children to miss school. Tadele & Hibistu (2021) Also, a large amount of grain is left on the stalk, poor quality of grain and unhealthy due to the mixture of dirt, stones, and animal dung. According to information gathered from the farmers, losses experienced before and after the harvest total to approximately forty percent of production loss Barretto et al. (2021). This is the reason why the country produces low yield and low quality Teff.

Pneumatic conveying is a widely used method for transporting bulk materials in various industries, including food, agricultural pharmaceuticals, and chemicals industries. Tadić et al. (2024) because it offers

many benefits over conventional mechanical conveyor systems, in recent years pneumatic conveyors have gained popularity as a grain handling solution because of their great adaptability, versatile handling application, used for different variety of grains, including moving grains over large distances, along curves, and even vertically. Improve efficiency and smooth integration is also possible since they are simple to incorporate into grain handling systems. Furthermore, the seamless integration and increased efficiency of pneumatic conveyors can be achieved with ease grain handling systems. According to this information, it has great advantage over mechanical conveyor to use a pneumatic conveying system for Teff grain, not only for transporting but also for panting cleaning and treatment. The study related to pneumatic Teff grain conveyors is crucial for the design and optimized pneumatic conveying system for Teff grain.

Khazaee (2017) cyclone separators are commonly used in pneumatic conveying systems due to their simplicity, efficiency, and low cost. In this process, a mixture of gas and solid particles is conveyed through a pipeline, and the particles are separated from the gas stream using a cyclone separator. Kaya & Karagoz (2012) cyclone separators are designed to separate grains from gas or to transport milled material, and their specific application and design may vary depending on the context and the materials being processed. The Lapple model is one of the most widely used models for predicting the performance of cyclone separators Wu et al. (2011) it is based on the principle of inertial impaction, where the particles are separated from the gas stream based on their size and inlet air velocity. Because of its simplicity, Demir (2014) the Lapple model to be effective in predicting the performance of cyclone separators in various applications.

A numerical study CFD-DPM methodology that evaluated square cyclone performance, adjusted parameters, and verified dependability was based on 3D CFD and Taguchi analysis Sommerfeld (2003).

Safikhani et al. (2020) studied the collision effects of turbulent gas-particle flow in a horizontal channel. The study shows wall roughness, fluctuating velocities, and particle dispersion cause inter-particle collisions. This study uses the Reynolds-averaged Navier-Stokes equations to demonstrate that a new design dynamic cyclone has higher efficiency and a lower pressure drop, with small particles yielding higher efficiency due to intensive rotation. It also examines the impact of inlet dimensions of cyclone, increasing inlet height and width and decreasing tangential velocity with limited variation in pressure and velocity Elsayed & Lacor (2012). Gimbun et al. (2005) According to the study, the most accurate model for estimating cyclone pressure drop under various operational conditions is the Lapple and Shepherd pressure drop model. By comprehensively studying the flow field, particle revolution, and self-rotation using DPM simulation, this work offered a unique way to strengthen particle self-rotation in cyclones through pre-self-rotation, improving cyclone separation theory and practice Fu et al. (2021). In order to estimate the separation efficiency of a rotating drum used to separate plastic granules with accuracy, this study built a CFD model. This model shed light on the applicability of rotating drums for the separation of plastics as well as the effects of air bubble attachments on the efficiency of separation Fatahian et al. (2023). Elsayed Khairy & Lacor (2010) this study employed computational fluid dynamics (CFD) and mathematical modeling to examine the impact of cyclone geometry elements on performance. With ratios comparable to Stairmand high efficiency design but better in terms of decreased pressure drop at a comparable cut-off diameter, the outcome was a new, improved cyclone design.

The literature review has identified a potential research gap in the experimental and CFD-DPM investigations of pressure drop for a pneumatic Teff grain conveyor system. While the existing studies have provided valuable insights into numerical CFD-DPM methodologies for assessing cyclone performance, cyclone design on efficiency and pressure drop, and the accuracy of pressure drop models, there appears to be a lack of specific research focused on the pressure drop characteristics of a pneumatic conveyor system handling Teff grains. To address this gap, the study involves experimental studies to determine the pressure drop in a Teff grain pneumatic conveyor system, coupled with the development and validation of CFD-DPM models to simulate the flow and pressure drop behavior. This combined experimental and numerical approach could provide a deeper understanding of the factors influencing pressure drop, such as particle characteristics, flow conditions, and conveyor design parameters. Additionally, as the literature review indicates, Lapple model could help identify the most suitable approach for predicting pressure drop in pneumatic conveyor systems.

The experimental approach involves conducting experiments in a laboratory setting to measure the pressure of the cyclone separator under different operating conditions. The experimental data is then used to validate the numerical model. For the numerical approach, CFD-DPM (Computational Fluid Dynamics-Discrete Phase Model) in ANSYS Fluent 17.2 is employed for simulation and analysis. The CFD-DPM model is also used to determine the pressure drop across the cyclone separator. The simulation results are then compared with the experimental data to develop a model that predict the real system behavior.

Validating the accuracy and reliability of a model through the comparison of simulation results and experimental data is essential, particularly for predicting the pressure drop in cyclone separators. By utilizing the Lapple model alongside experimental data and numerical simulations, this study aims to analyze the pressure drop in a pneumatic Teff grain conveying system. The findings are expected to significantly enhance the design and optimization of these systems, resulting in improved efficiency, cost savings, and better product quality.

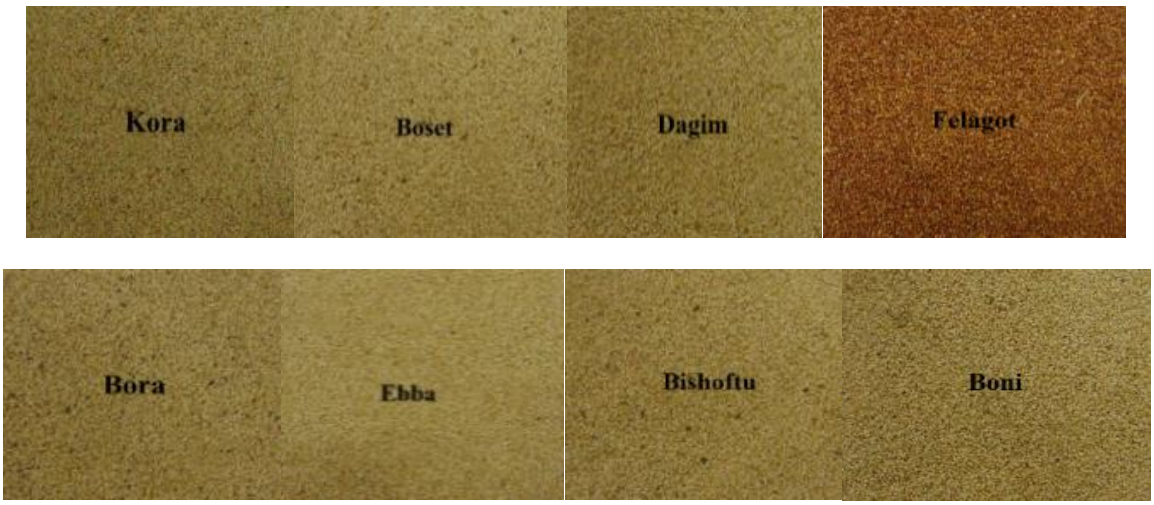

Fig. 1 Different varieties of Teff grain

Table 1 Summary of measured Teff grain size

Teff Variety	Width (mm)	Thickness (mm)	Length (mm)	Projected Area (mm^2)	Thousand Grain Weight(g)
Boset	0.63±0.05	0.56+0.10	1.01±0.13	0.50±0.07	292.44±42.93
Kora	0.68±0.10	0.57+0.06	1.09±0.18	0.58±0.12	297.46±462
Dagim	0.67±0.08	0.61+0.07	1.17±0.17	0.61±0.09	304.01±41.58
Felagot	0.52±0.07	0.52+0.08	0.92±0.08	0.42±0.06	251.82±14.38
Bora	0.58±0.09	0.56+0.04	1.10±0.18	0.50±0.11	276.57±38.15
Ebba	0.70±0.08	0.58+0.12	1.09±0.15	0.60±0.10	287.65±43.39
Bishoftu	0.59±0.14	0.54+0.08	0.94±0.15	0.44±0.12	279.39±36.47
Boni	0.59±0.09	0.53+0.03	0.94±0.15	0.44±0.12	287.42±43.63

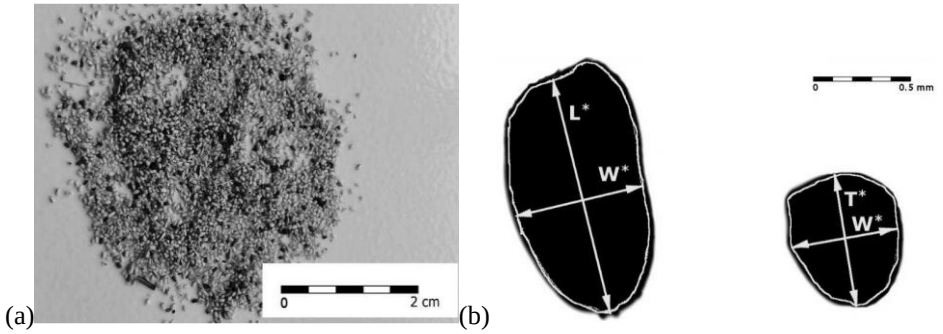

(a) (b)

Fig. 2 (a) Image of Teff grain (b) Dimension of grain

2. MATERIALS AND METHODS

2.1 Experimental Setup

Eight new varieties of Teff were collected according to the year of released such as Boset, Kora, Dagim, Felagot, Bora Ebba, Bishoftu, and Boni were obtained from Debre Zeit Agricultural Research Center of the Ethiopian Institute of Agricultural Research (EIAR). Those Teff varieties were released by the National Teff Improvement Program of the Ethiopian Institute of Agricultural Research (EIAR). The laboratory tests were conducted at Adama Science and Technology University, Chemical Department Laboratory.

Moisture content of eight different types of Teff grain measured according to ASAE standards S3523 (ASAE, 1994). Recorded moisture content for each variety of Teff grain is 9.14%-15%, 7.73%-13.48%, 10.14%-14.35%, 9.5%-15.28%, 11.59%-14.14%, 9.5%-13.36%, 10.25%-12.36%, and 8.65%-11.96% for Felagot, Ebba, Bishoftu, Dagim, Boni, Boset, Kora, and Bora, respectively.

Particle size distribution of dimensions 20 pieces of Teff seeds were used where dimensions of each seeds: length L (mm), width W (mm), thickness T (mm), were determined by digital image analysis using ImageJ software from pictures which were taken with the aid of a trio ocular microscope Asefa et al. (2023). Geometric mean diameter D_g=0.68mm and arithmetic mean diameter D_a= 0.72mm.

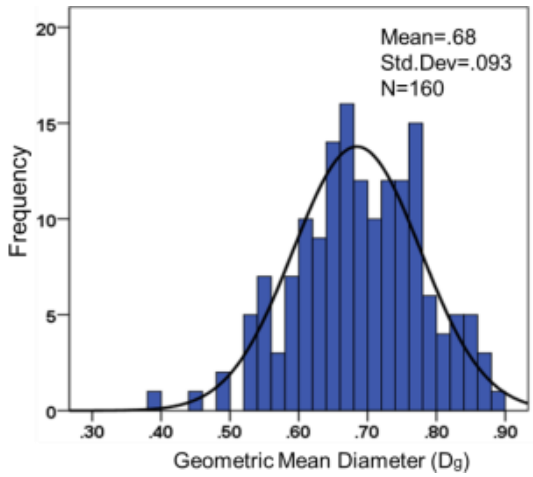

(a)

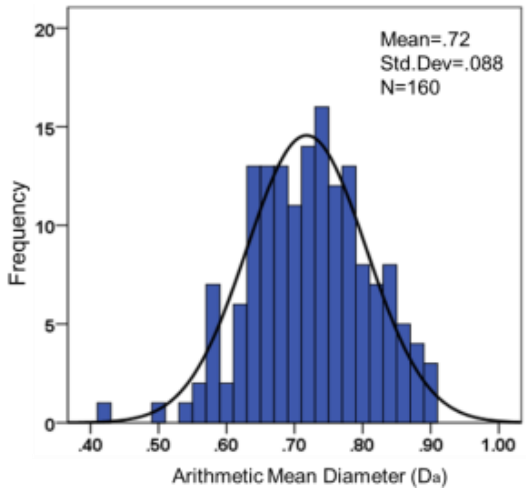

(b)

Fig. 3 a) Geometeeric mean diameter b)arithmetic mean diameter

Geometric mean diameter D_g(mm) and Arithmetic mean diameter D_a(mm) calculated using the following equation.

$$D_g = \sqrt[3]{W \times T \times L} \tag{1}$$

$$D_a = \frac{W + T + L}{3} \tag{2}$$

Experimental investigation was used to determine pressure drop across cyclone separators in pneumatic conveyor Teff grain systems. The study utilized the Lapple cyclone separator model and examined the effects of varying cyclone sizes 0.75D, 0.9D, and 1D for D=200mm, inlet air velocity 10m/s, 14m/s, 18m/s, 22m/s, and material mass flow rate 0.009kg/s, 0.03kg/s, 0.044kg/s, 0.067kg/s.

The laboratory conducted precise measurements of inlet air velocity and pressure drop using advanced instrumentation. GM816 Professional digital anemometer was employed to measure the air velocity at the inlet with a resolution of 0.1 m/s and MAN-45 Professional digital manometer was utilized to record pressure drop, with a resolution of 0.01 kPa. These measurements are crucial

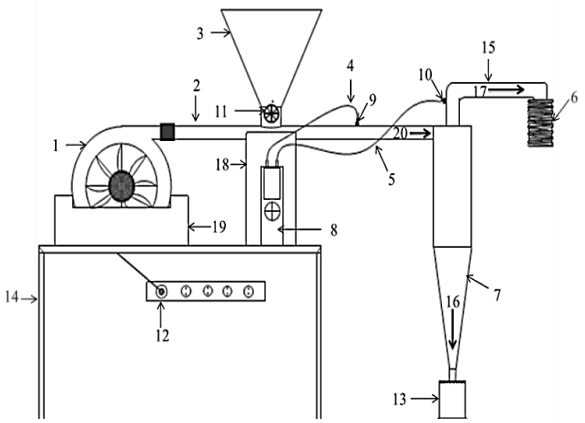

Fig. 4 Cyclone separator setup for experimental test 1: blower; 2: inlet pipe; 3: hopper; 4 and 5: hose; 6: dust collector; 7: cyclone; 8: digital manometer; 9 and 10: hose pipe connector; 11: valve; 12: power source; 13: Teff grain collector; 14: table; 15; outlet pipe; 16: Teff grain outlet; 17: air outlet; 18: blower holder; 19: system support; and 20: inlet

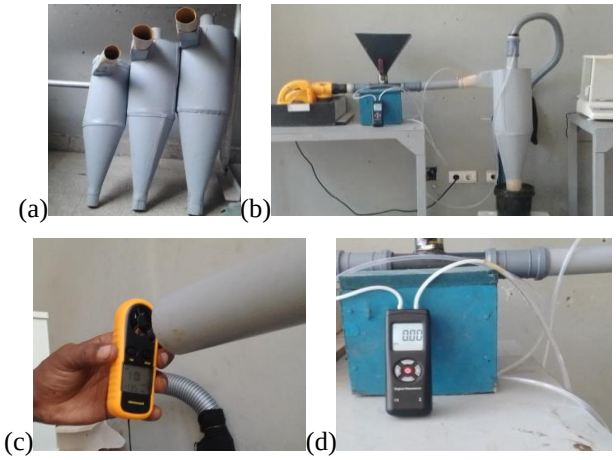

Fig. 5 Laboratory experiment involves (a) cyclone for laboratory test, (b) Laboratory setup (c) Air velocity measuring using digital anemometer, and d) pressure drop measuring using digital manometer

as they provide insights into the airflow measurement and pressure difference and efficiency of the cyclone system being tested. By varying both the air flow rate and mass flow rate, the laboratory recorded the pressure drop, defined as the difference in pressure between the inlet and outlet of the cyclone. The data collected from these experiments contribute to a better understanding of the cyclone's separator operational efficiency and to validate the numerical study.

2.2 Numerical Analysis

Multiphase modeling in CFD can be done in many ways. Most commercial software allows modeling any combination of solid, liquid, and gas in pairs or all three at once. Ghafori and Sharifi (2018), it is also not uncommon to have more than one constituent of a phase present in a single simulation, an example being two different solid materials being transported by a liquid or

Table 2 Geometry of the cyclone separator for (D=150mm, 180mm and 200mm)

Cyclone diameter (D)	W	L_b	L_c	H	D_e	D_d	S	L_b+ L_c
	0.25D	2D	2D	0.5D	0.5D	0.25D	0.625D	4D
0.15m	0.037	0.3	0.3	0.075	0.075	0.037	0.093	0.6
0.18m	0.045	0.36	0.36	0.09	0.09	0.045	0.112	0.72
0.2m	0.05	0.4	0.4	0.1	0.1	0.05	0.125	0.8

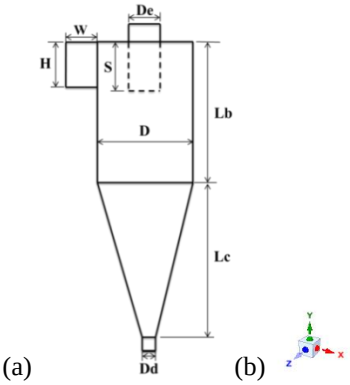

(a) (b)

Fig. 6 (a) 2D drawing for geometry of cyclone (b) 3D modeling for cyclone ANSYS R17.2

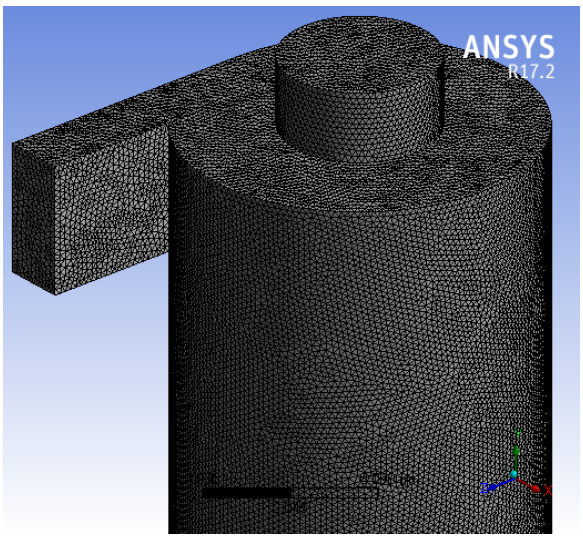

Fig.7 ANSYS 17.2 mesh window at D=200mm and mesh size=2.72mm

gas. According to Ma et al. (2010), multiphase modeling can be performed in an Euler-Euler or Euler-Lagrange framework. The main model used in Fluent under the Euler-Lagrange umbrella is called the Discrete Phase Model or DPM Singh et al. (2023). The number of iterations used for this study ranges from 500 to 1000. As the scaled residuals approach zero, or when the targeted residuals fall below the specified values, we observed that the simulation converges immediately in most cases. In some simulations, convergence occurs below the iteration number of 500, and in some simulations, increasing the number of iterations beyond 500 to 1000 results in convergence, and all simulations fall within this range.

In CFD-DPM simulation, number iteration depends up on scaled residuals. When scaled residuals approach to zero and less than (1E-5)-(1E-6) the simulation became converged. The equations used to compute the trajectory of the discrete phase particle is given as follows:

$$\frac{du_p}{d_t} = Fd(u-u_p) + \frac{g(\rho_p-\rho)}{\rho_p} + F \tag{3}$$

Where u_p and u are the particle and fluid velocities, respectively, ρ_p and ρ are the particle and fluid densities, respectively. The drag force, F_d, acting on a spherical particle is

$$F_d = \frac{18\mu C_D \,\mathrm{Re}}{\rho_p d_p^2 24} \tag{4}$$

Where Re is the Reynolds number, μ is the dynamic viscosity of the fluid, and C_D is the drag coefficient based on the shape of the particle Cao et al. (2022).

2.3 Turbulence Model

Reynolds values greater than 2300 for internal cyclone separators indicate the presence of turbulence, which needs to be taken into consideration in the momentum balance. Because of the high velocity and low viscosity of the air in the pneumatic conveying systems, Huang et al. (2021) Reynolds numbers are consistently significantly higher than 2300. The mass and momentum transport equations have the following Reynolds- and time-averaged forms:

$$\frac{\partial \rho}{\partial t} = \nabla.(\rho\vec{v}) = S_m \tag{5}$$

$$\frac{\partial \rho}{\partial t} + \nabla\rho(\vec{v}.\vec{v}) = \nabla.p + \nabla\bar{\bar{T}} + \nabla\rho(\overline{\vec{v}'.\vec{v}'}) + \rho\vec{g} + \vec{F} \tag{6}$$

Re-Normalization Group, or RNG, is the model used in the k-ε formulation. It is obtained by applying the renormalization statistical approach to the instantaneous conservation equations. A term added to the ε transport equation improves the prediction of rapidly strained and swirling flows, and an analytical expression for the Prandtl numbers replaces the standard model's previously used constant numbers Wang et al. (2023). These are the main ways in which the RNG model differs from the standard model. The RNG model is generally more trustworthy than the conventional k-ε model due to these enhancements. In order to apply the k - ε method, the transport equations must be solved Dutta et al. (2016).

$$\frac{\partial \rho k}{\partial t} + \nabla\rho(k.\vec{v}) = \nabla.(\mu + \frac{\mu_T}{\sigma_k} * \nabla k) + G_k + G_k + \rho\varepsilon + Y_M + S_k \tag{7}$$

$$\frac{\partial \rho \varepsilon}{\partial t} + \nabla\rho(\varepsilon.\vec{v}) = \nabla.(\mu + \frac{\mu_T}{\sigma_\varepsilon} * \nabla\varepsilon) + C_{1\varepsilon}\frac{\varepsilon}{k} + (G_k + C_{3\varepsilon}G_b) - C_{2\varepsilon}\rho\frac{\varepsilon^2}{k} + S_\varepsilon \tag{8}$$

Table 3 CFD-DPM setup

CFD-DPM Setup	
Geometry Modeling	ANSYS Space Claim 2024R1 geometry modeler to create a 3D geometry model, Dimensions of the model: 0.75D, 0.9D, and 2D, where D = 200 mm
Mesh Generation	Mesh size to particle mean diameter ratio should be greater than 4 and Mesh size for this study is set to 4.5E-3 m
Particle Properties	Teff grain mean diameter (d_p) = 68E-4 m Minimum diameter = 54E-4 m Maximum diameter = 82E-4 m Particle material mass flow rates: - 0.009 kg/s - 0.03 kg/s - 0.044 kg/s - 0.067 kg/s Particle shape factor = 0.76 (non-spherical particle) Particle density (ρ_p) = 1120 kg/m^3
Fluid Properties	Air density (ρ_a) = 1.225 kg/m^3 Air viscosity = 1.7894E-05 kg/m•s
Operating Conditions	Gravitational acceleration (g) = -9.81 m/s^2 along the y-axis
Discrete Phase Model	Two-way coupling: Interaction with continuous phase Turbulence model: - k-ε - RNG - Swirling dominated - Standard wall functions Injection type: Surface injection through the inlet Particle diameter distribution: Rosin-Rammler model Particle physical model - Non-spherical particle drag law - Shape factor: 0.76
Boundary Conditions	Inlet surface: - Air velocities: 10 m/s, 14 m/s, 16 m/s, 18 m/s, 22 m/s (in the Z-axis) Interior volume Outlet surface: - Gas outlet escape - Solid material outlet escape - Outlet pressure: 0 Pa Wall solid: - Wall reflect
Solution Method	Pressure-Velocity Coupling: SIMPLE Discretization Schemes: - Pressure: Second Order - Momentum: Second Order Upwind - Turbulence Kinetic Energy: Second Order Upwind - Turbulence Dissipation Rate: Second Order Upwind - Discrete Phase: Second Order Upwind
Run calculation	Number of iterations: 500 - 1000 Reporting interval=1 Profile update interval=1
Convergence Criteria	Residual Targets: - Continuity: 1E-5 - Velocities: 1E-6 - Turbulence Quantities: 1E-6 - Discrete Phase: 1E-5
Report File Definition	Area weighted - Average static pressure (Pa) Detailed Fluent PT for pressure and velocity distribution

Where Y_M accounts for compressibility effects on turbulence, G_k is the generation of turbulence due to the velocity gradients (local strain), G_b is the generation of turbulence due to buoyancy effects, and σ_k and σ_ε are the turbulent Prandtl numbers for k and ε.$C_{1\varepsilon}$, $C_{2\varepsilon}$, $C_{3\varepsilon}$ and in

the dissipation rate equation are constants that are derived by calibration with experiments, and S_k and S_ε are user defined source terms. The local solution for k - ε enables calculation of the local eddy viscosity, which takes the form: $\mu_T = \rho C_\mu k^2/\varepsilon$. Singh et al. (2023) the eddy viscosity appears in the momentum equations and in the k and ε equations so the solution procedure is strongly coupled.

2.4 CFD-DPM ANSYS Fluent simulation setup

Teff grain is non-spherical particle and exhibit a particle size distribution due to the natural variability in seed size. In CFD-DPM simulation, accurately representing the behavior of non-spherical particles with size distributions is crucial for obtaining reliable results. Modeling approaches used for the study, such as the non-spherical particle with a shape factor= 0.76 and Rosin-Rammler particle diameter distribution model Roberts et al. (2022). To capture the turbulent effects, k-ε RNG swirling dominated turbulence model was used for this study. For pressure and velocity coupling, the simple solution approach with a pressure-based solver was employed. Xu et al. (2024) the discretization of momentum, turbulence kinetic energy, and turbulence dissipation rate equations was done using second-order upwind schemes. Dutta et al. (2016) the pressure drop across the cyclone separator computed using the CFD results from the surface integral result for area weighted average static pressure and pressure drop calculated from difference between static pressure at the inlet and outlet. After completing a simulation that meets convergence criteria, particle data can be exported to CFD Post. This powerful tool allows for detailed visualization of pressure distribution and particle velocity profiles, enhancing the understanding of fluid dynamics and improving system optimization.

The injection duration (t) is the time period over which particles are injected in a CFD-DPM simulation. It is one of the key parameters used to calculate the number of injected particles.

$$N = \frac{m_s \times t}{m_p} \tag{9}$$

Where: N = Number of particles to inject, m_s = Mass flow rate of the particles (kg/s), t = injection duration (s) and m_p= Mass of a single particle (kg).

In the DPM injection settings, the injection duration is specified along with the start time; for instance, to inject particles from t = 0 to t = 1 second, set the start and stop times to 0 and 1 seconds, mass of a single Teff grain m_p= 0.000286 (as indicated in Table 1), number of particles injected for various mass flow rates is as follows: for m_s=0.009 kg/s, N=320; for m_s=0.03kg/s, N=505; for m_s=0.044kg/s, N=654; and for m_s=0.067kg/s, N=836.

Determination of pressure drop in a cyclone separator using CFD simulation typically employs a two-way coupling approach, which accounts for the interaction between particles and the continuous phase. In this context, the boundary condition for the walls is set to reflect. This reflect boundary condition means that when a particle collides with a solid surface, it is reflected back into the computational domain rather than being absorbed or passing through the boundary.

It is advised to keep the mesh size at least four times larger than the particle size in CFD-DPM simulations with the k-ε turbulence model. By maintaining this ratio, the mesh is guaranteed to be sufficiently coarse to accurately resolve the particle motion and represent the bulk flow behavior Cao et al. (2022). Furthermore, it is important to keep the non-dimensional wall distance (Y+) for the k-ε turbulence model between 30 and 300. This Y+ range relates to the boundary layer's log-law region, where the k-ε model is applicable and capable of correctly predicting the turbulent flow close to solid boundaries Dutta and Nandi (2019).

For CFD-DPM simulations, mesh sensitivity analysis is carried out to guarantee grid-independent outcomes and precise pressure drop predictions across cyclone separators. This is accomplished by creating several mesh models with different levels of resolution, simulating CFD-DPM for each mesh, and tracking the pressure decrease as the mesh gets more and more accurate. A coarse mesh is used for the study at first, and when it is refined, the pressure decrease that results is noted. The pressure drop curve is refined until it either forms a flat plateau or becomes invariant. In the CFD-DPM simulation, the mesh size is set to be at least four times larger than the particle size, as the mean diameter of the Teff grain is 0.68 mm. The mesh size range for this investigation starts from the finest mesh size of 2.72 mm to the coarsest mesh size of 10 mm.

The Fig. 8 (a) is indicated that pressure drop curve having a flat section, which shows that more mesh refinement, has no effect on the solution. The mesh refinement flat curve procedure ranges from 6.25 mm to 2.72 mm with a midpoint value of 4.5 mm traced and corresponding Y+ value of 97.16 has been obtained, Fig.8 (b) Y-plus for mesh size = 4.5mm. In order to guarantee precision and uniformity in the CFD-DPM analysis, a mesh size of 4.5 mm is chosen for every following simulation.

3. RESULTS AND DISCUSSIONS

In this study, we investigate the pressure drop across a cyclone separator within a pneumatic conveying system specifically designed for Teff grain, utilizing a combination of experimental measurements and CFD-DPM simulations. The experimental setup is designed to employ a digital anemometer to accurately measure the inlet air velocity, while a digital manometer is utilized to record the pressure drop across the cyclone separator. To effectively capture the complex flow dynamics within the cyclone, the k-epsilon RNG swirling-dominated turbulence model is employed in the simulations, which is a well-suited turbulent model for handling complex flow characteristics throughout the cyclone separator. This comprehensive approach aims to enhance our understanding of the pressure drop behavior in cyclone separators and provide valuable information for

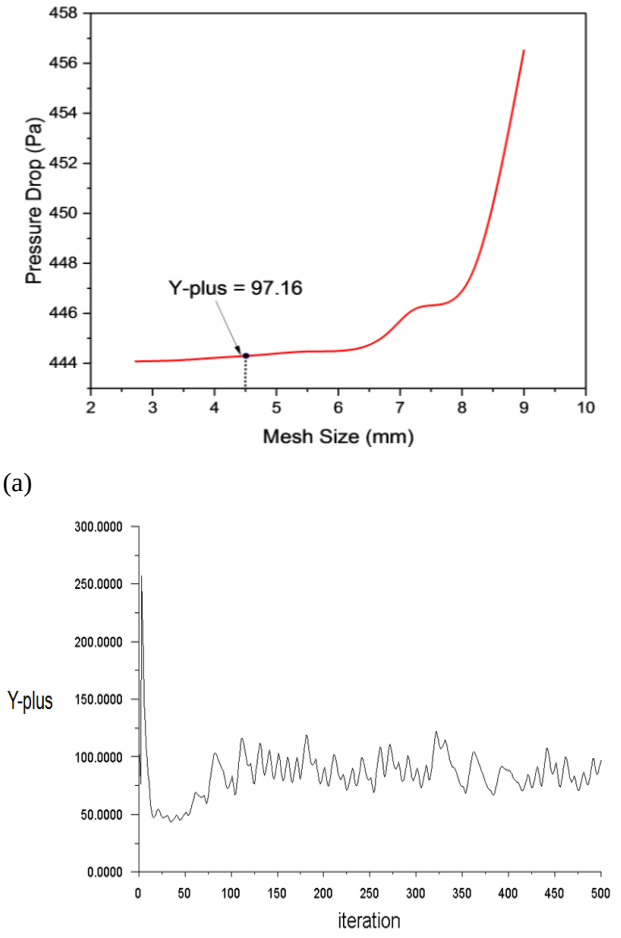

Fig. 8 (a) mesh size vs. pressure drop (b) Y-plus

the optimization of the pneumatic Teff grain conveying system.

Figure 9(a & b)–11(a & b) shows the findings from both experimental investigations and simulation results, which collectively indicate that as the solid mass flow rate and inlet air velocity increase, the pressure drop throughout the cyclone separator also increases. This phenomenon can be attributed to the enhanced particle velocity and particle fluid interaction, which increase swirling motion within the cyclone separator. The increased swirling motion leads to a greater pressure drop. Furthermore, the results emphasize that there is a significant impact of cyclone separator size on pressure drop. When the size of the cyclone separator decreases, pressure across the separator rises. This can be explained by faster particle flow, which leads to more swirling motion within the smaller cyclone. In both cases, the result highlights the importance of considering the interplay between inlet air velocities, solid mass flow rate, and cyclone separator size when designing and optimizing pneumatic Teff grain conveying systems. The combination of experimental data and simulation results provides a comprehensive understanding of the complex fluid dynamics within cyclone separators, enabling informed decision-making in the development of efficient and reliable pneumatic Teff grain conveying.

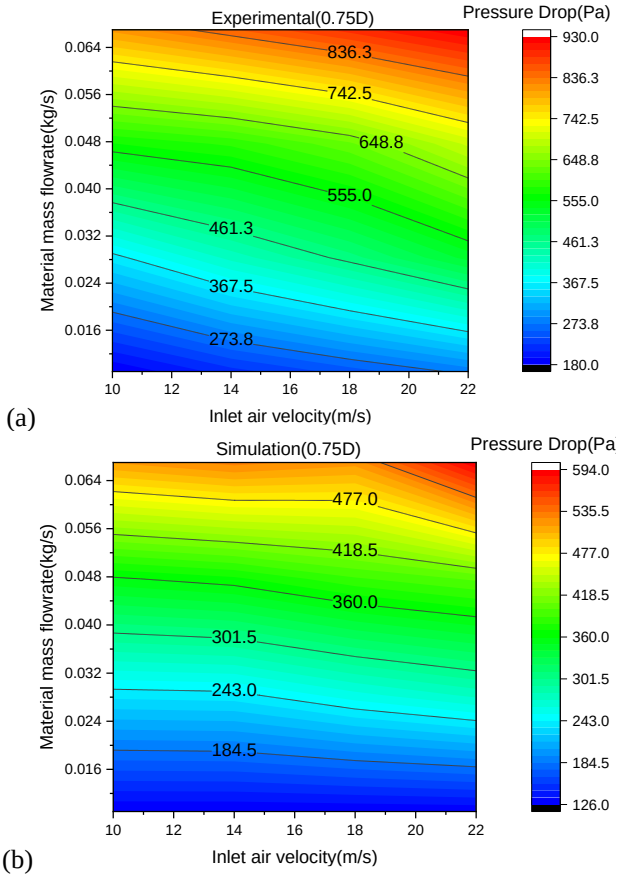

Fig. 9 (a) Experimental and (b) simulation pressure drop for 0.75D cyclone

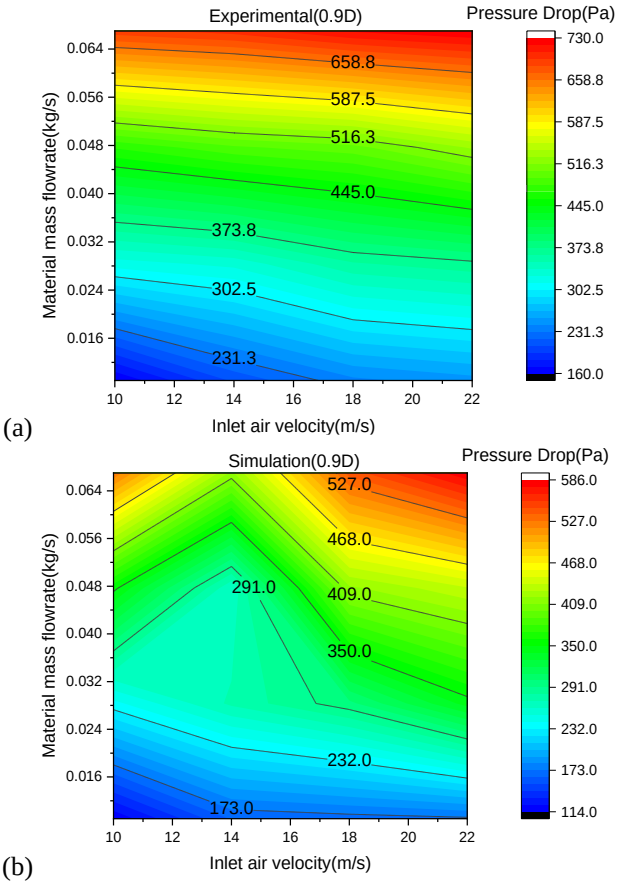

Fig. 10 (a) Experimental and (b) simulation pressure drop for 0.9D cyclone

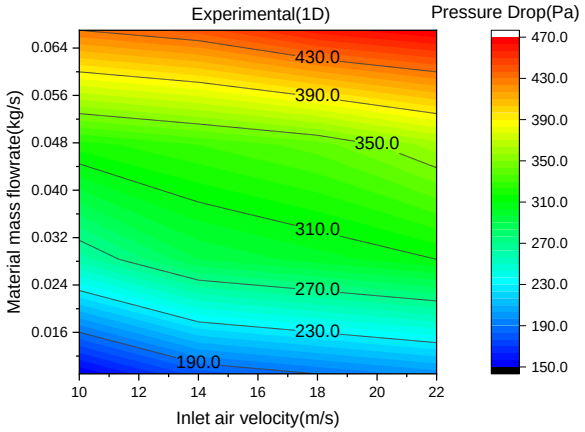

Fig. 11 (a) Experimental and (b) simulation pressure drop for 1D cyclone

In Figs. 12 and 13, the CFD-DPM method in ANSYS Models with the k-ε RNG swirling-dominated turbulent flow model shows that the pressure drop and particle velocity across the cyclone rise with increasing inlet air velocity and solid mass flow rate, according to the CFD-POST Fluent PT of Teff Grain pressure drop and velocity distribution results. This is because in the cyclone's high turbulence gas flow is causing a swirling dominant flow. On the other hand, when the cyclone size decreases, the pressure drop and particle velocity increase because the solid and gas particles have a smaller cross-sectional area and are moving faster.

3.1 Determination of Pressure Drop Coefficient

The pressure drop across a cyclone essentially depends on the cyclone dimensions and operating conditions. Zhao (2009), (Demir, 2014) generally, it is proportional to the gas inlet velocity head and is often defined as:

$$\Delta P = \frac{1}{2}\rho_g v_i^2 N_H \tag{10}$$

Where, ΔP is cyclone pressure drop, ρ_g is gas density, v_i is inlet velocity, and N_H is a number of velocity heads, and it is a pressure drop parameter to account for all pressure drop components in terms of inlet velocity heads.

$$N_H = 16\frac{WH}{D_e^2} \tag{11}$$

The number of velocity heads (N_H) is also referred to as the pressure drop coefficient for a cyclone separator, as it is a dimensionless parameter that quantifies the pressure drop across the cyclone.

Multi-regression analysis was used to determine the relationship between pressure drop, inlet air velocity and cyclone diameter. Regression data assumptions were analyzed, and solid mass flow rate has no significant effect on pressure drop; cyclone dimension and inlet air velocity have highly significant effects on pressure drop. The regression equation is expressed as below:

$$y = b_1 x_1 + b_2 x_2 + c \tag{12}$$

Where y=dependent variable, x_1 and x_2 are independent variables, b_1 and b_2 coefficients and c constant, and expressed in terms v = inlet air velocity and D=cyclone diameter.

$$y = b_1 v + b_2 D + c \tag{13}$$

Pressure drop coefficient N_H for experimental: b_1= -0.1038, b_2= -25.691 and c= 9.109, and for simulation: b_1= -0.58, b_2= -13.75 and c= 5.424.

$$N_H = -0.1038v - 25.691D + 9.109 \tag{14}$$

$$N_H = -0.58v - 13.75D + 5.424 \tag{15}$$

The pressure drop coefficient for equation (14) is N_H calculated for the experimental result, and equation (15) is N_H calculated for the simulation result.

Regression analysis shows that inlet air velocity and cyclone size have a significant effect on pressure drop across the cyclone separator, and the material flow rate has no significant effect on the pressure drop across the cyclone separator. This analysis is used to express the relationship between the influential variables to estimate pressure drop across cyclone separators under different operating conditions.

Figure 14 (a) and (b) show a strong correlation between the results obtained from CFD-DPM simulations and the experimental data related to pressure drop across a cyclone separator in a pneumatic Teff grain conveying system. Both figures illustrate the model's ability to replicate real-world conditions closely. The correlation is quantitatively reinforced by an impressive R-squared value of 0.99, indicating that the CFD-DPM simulations can explain 99% of the variance in the experimental results. This high degree of correlation suggests that the model is highly reliable for predicting pressure drops in this context. Additionally, the residual sum of squares (RSS) of 38.018 further emphasizes the accuracy of the CFD-DPM model, reflecting minimal deviation between the simulated and experimental data. Overall, these findings validate the effectiveness of CFD-DPM in modeling cyclone separator performance in grain conveying systems.

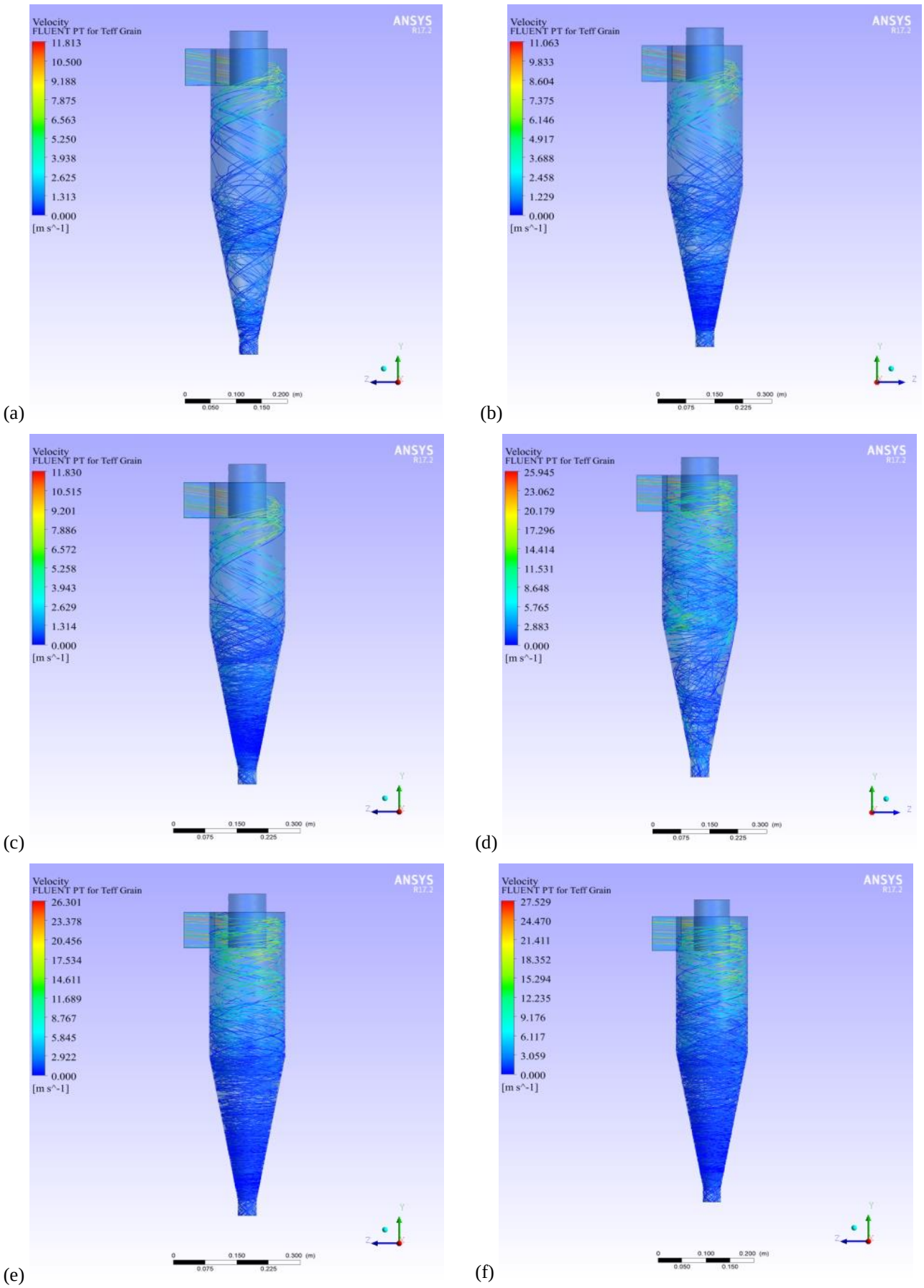

Fig.12 (a-c) minimum pressure distributions at 10m/s and 0.009kg/s, (d-f) maximum pressure distributions at 22m/s and 0.067kg/s for 0.75D, 0.9D and 1D cyclones

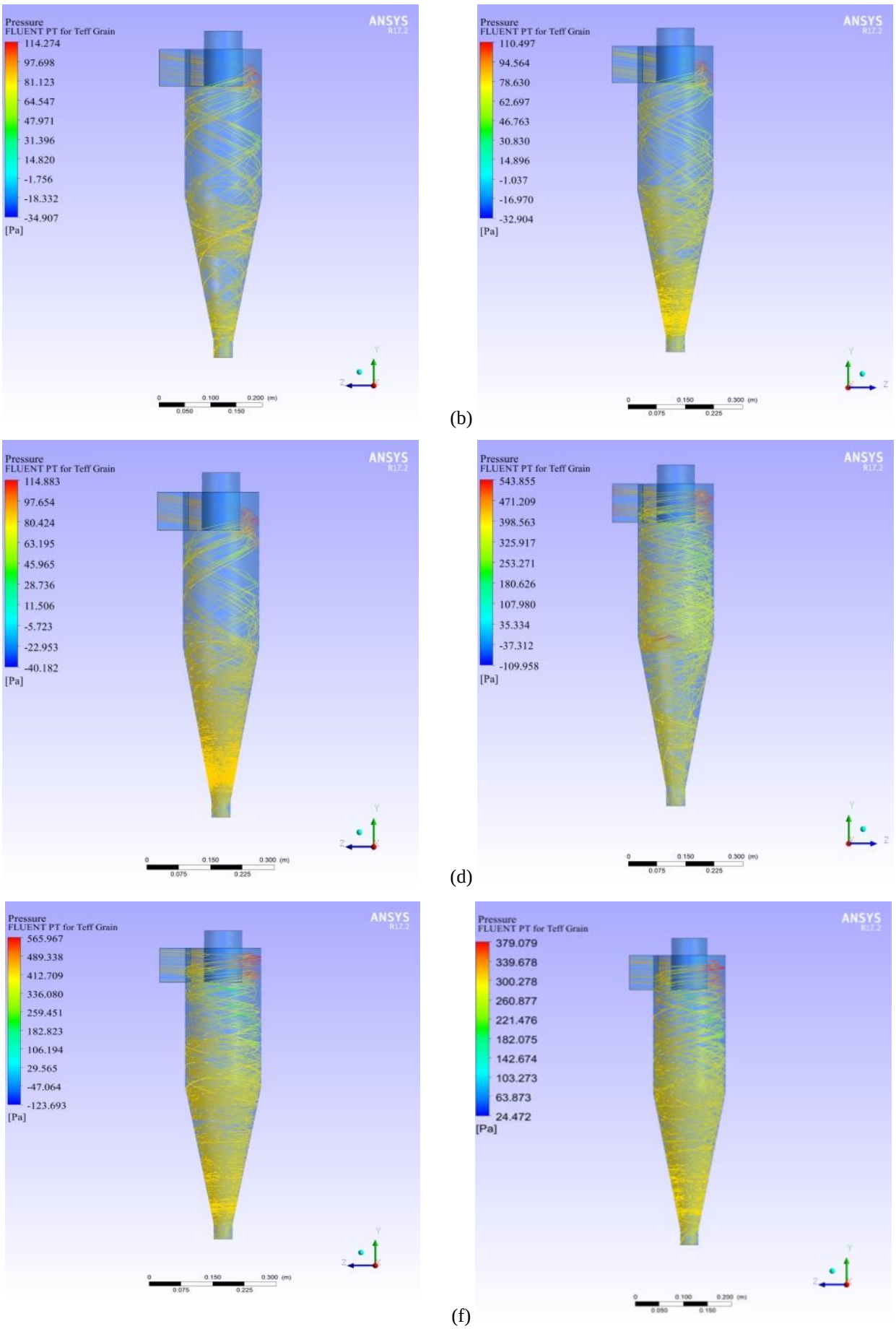

Fig. 13 (a-c) minimum particle velocity profile at 10m/s and 0.009kg/s, (d-f) maximum particle velocity profile at 22m/s and 0.067kg/s for 0.75D, 0.9D and 1D cyclones

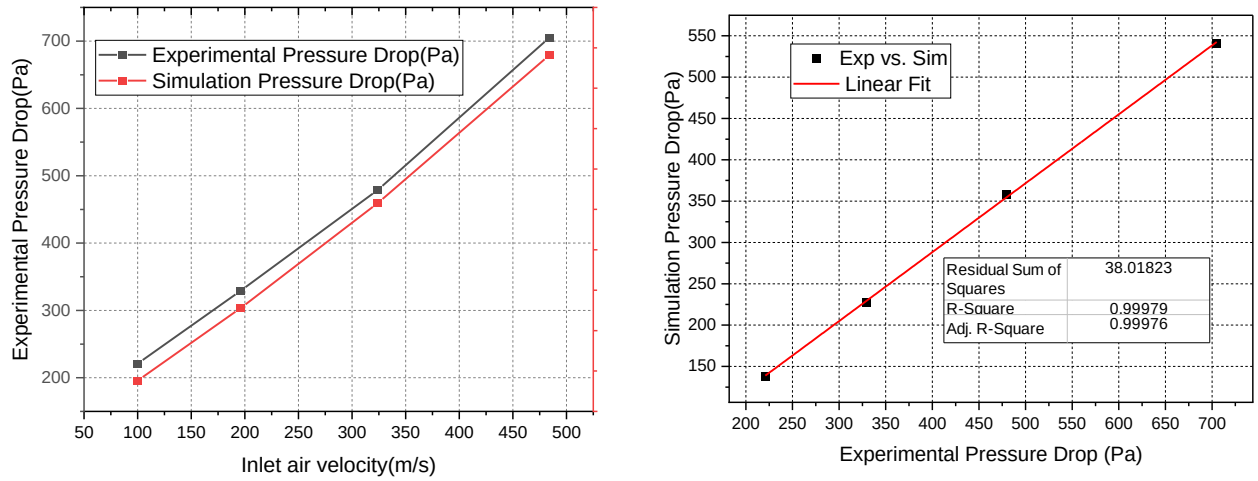

(a) (b)

Fig. 14 (a) pressure drop vs. inlet air velocity and (b) Experimental vs. simulation pressure drop

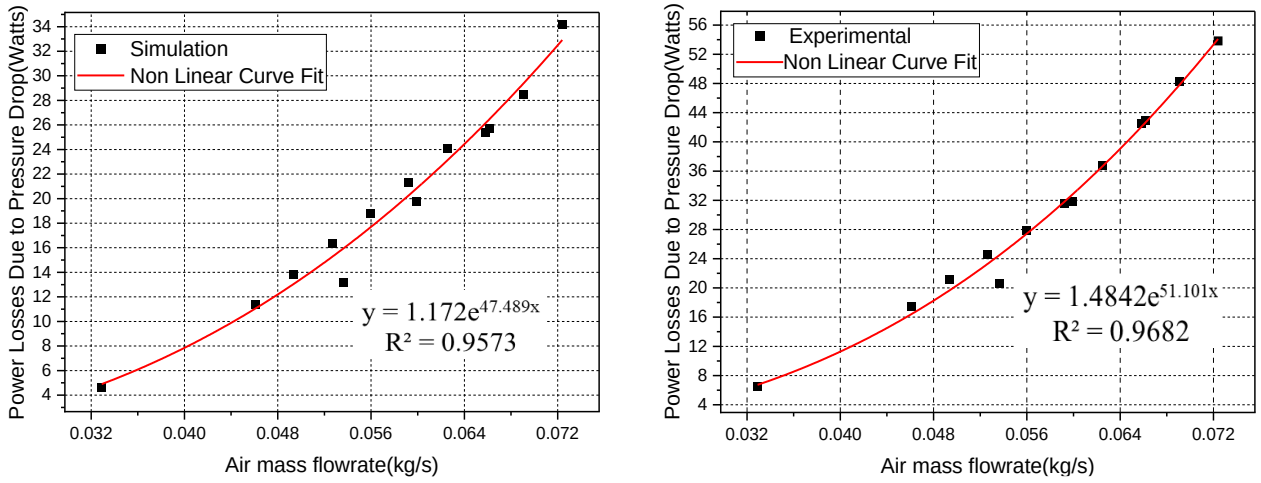

(a) (b)

Fig. 15 (a) and (b): Power losses vs. Air mass flow rate

Figure 15 (a) and (b) illustrate that as both air mass flow rate and material flow rate increase, there is a corresponding rise in the pressure drop across the cyclone separator in the pneumatic Teff grain conveying system. This relationship highlights the direct impact of flow rates on system performance, as higher pressure drops lead to increased power losses within the system. The increased power losses are a critical consideration for system efficiency. Furthermore, by utilizing the equation derived from the fitting curve, we can accurately calculate the power losses associated with air mass flow rates and material mass flow rates. This calculation is essential for optimizing system design and operation, enabling engineers to make informed decisions that enhance efficiency and reduce energy consumption in pneumatic Teff grain conveying systems.

Pressure drop results across cyclone separators show that in Fig. 15, there is a strong alignment between experimental findings and CFD-DPM results, while a significant divergence exists between the Lapple model and experimental data. The Lapple model, which only

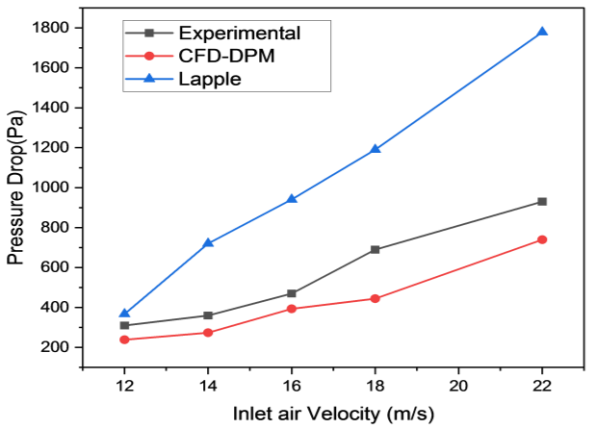

Fig. 15 Comparison of experimental, CFD-DPM and Lapple model

takes into account gas characteristics and the number of velocity heads, it has lacks depth to account for complex flow in cyclone separators, whereas the CFD-DPM

approach effectively captures complex flow dynamics and particle behavior within cyclones under various operating conditions, making it a superior method for predicting pressure drop in cyclone separators.

3.2 Energy Costs Analysis

In Ethiopia, the capacity of some small-scale Teff mills that use simple mechanical grinders powered by electricity or diesel engines is around 10,000 kg of Teff per day; the air flow rate through the cyclone is 0.035 m^3/s; the measured cyclone pressure drop is 1,800 Pa; and the current electricity cost is $0.0045 per kWh.

Energy cost of pressure drop:

Power needed to overcome pressure drop = Pressure drop x Air flow rate

Power (Watts) = 1,800 Pa x 0.035 m^3/s

Power = 0.632 kW

Energy cost per day = Power x Operating hours x Electricity cost

Energy cost per day = 0.632 kW x 24 hours x $0.0045/kWh

Energy cost per day = $0.0682 per day

Benefits of efficient cyclone separation:

Cyclone separation improves Teff yield by 2% Teff price is $1.25 per kg.

Increased revenue per day = 2% x 10,000 kg x $1.25/kg Increased revenue per day = $250 per day

Reduced post-processing costs (estimated 10% reduction) = $50 per day

Net benefit per day = Increased revenue + Reduced costs - Energy cost

Net benefit per day = $250 + $25 - $0.0682

Net benefit per day = $274.93 per day

This analysis shows that the benefits of efficient cyclone Teff grain separation, in terms of increased yield and reduced post-processing costs, can outweigh the energy costs associated with the pressure drop. The net daily benefit of over $274.93 highlights the practical and economic advantages of optimizing cyclone performance for Teff processing operations.

The present investigation aims to investigate the pressure loss caused in a pneumatic Teff grain conveyor system through a cyclone separator. The main aims of this study are to investigate the pressure drop through the cyclone separator using experimental and CFD-DPM methodologies. Additionally, an energy cost analysis will be carried out to evaluate the pressure drop's economic consequences. The CFD-DPM method used in the study does not fully account for variations in particle shape, density, and moisture content and the results may not be relevant to other cyclone models because the study is only focused on the Lapple cyclone model. In addition, in CFD-DPM simulation, one significant limitation is its inability to effectively account for particle-particle interactions, particularly at high solid loading ratios. The study recommends that future studies focus on comparing different cyclone models and consider variations in size, density, shapes, and the effects of particle-particle interactions on cyclone separator performance.

4. CONCLUSION

The findings show that pressure drop through a cyclone separator is highly affected by inlet air velocity and cyclone size. Higher inlet velocities lead to greater centrifugal forces acting on particles, which in turn increases pressure drop, and smaller cyclones have a higher surface-to-volume ratio, resulting in greater frictional losses and higher pressure drop.

There is a strong correlation between CFD-DPM results and experimental findings, but there is a notable difference between the Lapple model and experimental results. Lapple model considers the gas properties and number of velocity heads, but it isn't as comprehensive in its analysis of the particle-cyclone interaction as the CFD-DPM method, which is a better way to predict pressure drop across cyclone separators because it captures complicated flow dynamics and particle behavior within cyclones under different operating conditions.

The energy cost analysis shows that the benefits of efficient cyclone Teff grain separation, in terms of increased yield and reduced post-processing costs, can outweigh the energy costs associated with the pressure drop. The net daily benefit highlights the practical and economic advantages of optimizing cyclone performance for Teff processing operations.

ACKNOWLEDGEMENTS

Adama Science and Technology University's head of mechanical engineering department offered the laboratory needed for the study.

CONFLICT OF INTEREST

There are no possible conflicts of interest that the author(s) have disclosed about the research, writing, or publication of this article.

AUTHORS CONTRIBUTION

Lemi Demissie: Conceptualization, Investigation, reviewing, Writing original draft, and Editing; **Zewdu Abdi:** Conceptualization, Analysis, Visualization, and Supervision; **Amana Wako:** Analysis, Reviewing, and Supervision.

REFERENCE

Asefa, B. G., Tsige, F., Mehdi, M., Kore, T., & Lakew, A. (2023). Rapid classification of tef [Eragrostis tef (Zucc.) Trotter] grain varieties using digital images in combination with multivariate technique. *Smart*

Agricultural Technology, *3*(July). https://doi.org/10.1016/j.atech.2022.100097

Barretto, R., Buenavista, R. M., Rivera, J. L., Wang, S., Prasad, P. V., & Siliveru, K. (2021). Teff (Eragrostis tef) processing, utilization and future opportunities: a review. *International Journal of Food Science & Technology*, *56*(7), 3125-3137. https://doi.org/10.1111/ijfs.14872

Cao, L., Zhang, Q., & Meng, R. (2022). CFD–DPM simulation study of the effect of powder layer thickness on the SLM spatter behavior. *Metals*, *12*(11). https://doi.org/10.3390/met12111897

Demir, S. (2014). A practical model for estimating pressure drop in cyclone separators: An experimental study. *Powder Technology*, *268*, 329–338. https://doi.org/10.1016/j.powtec.2014.08.024

Dula, M. W. (2016). Development and evaluation of teff threshing machine. *International Journal of Engineering Research and Technology* *5*(11), 420–429. https://doi.org/10.17577/ijertv5is110250

Dutta, P., & Nandi, N. (2019). Numerical study on turbulent separation reattachment flow in pipe bends with different small curvature ratio. *Journal of The Institution of Engineers (India): Series C*, *100*(6), 995–1004. https://doi.org/10.1007/s40032-018-0488-9

Dutta, P., Saha, S. K., Nandi, N., & Pal, N. (2016). Numerical study on flow separation in 90° pipe bend under high Reynolds number by k-ε modelling. *Engineering Science and Technology, an International Journal*, *19*(2), 904–910. https://doi.org/10.1016/j.jestch.2015.12.005

Elsayed Khairy, K., & Lacor, C. (2010). Optimization of the cyclone separator geometry for minimum pressure drop using mathematical models and CFD simulations. *Chemical Engineering Science*, *65*(22), 6048–6058. https://doi.org/10.1016/j.ces.2010.08.042

Elsayed, K., & Lacor, C. (2012). Modeling and pareto optimization of gas cyclone separator performance using Rbf type artificial neural networks and genetic algorithms. *Powder Technology*, *217*, 84–99. https://doi.org/10.1016/j.powtec.2011.10.015

Fatahian, H., Fatahian, E., & Erfani, R. (2023). Square cyclone separator: performance analysis optimization and operating condition variations using CFD-DPM and taguchi method. *Powder Technology*, *428*(June), 118789. https://doi.org/10.1016/j.powtec.2023.118789

Fu, P., Zhu, J., Li, Q., Cheng, T., Zhang, F., Huang, Y., Ma, L., Xiu, G., & Wang, H. (2021). DPM simulation of particle revolution and high-speed self-rotation in different pre-self-rotation cyclones. *Powder Technology*, *394*, 290–299. https://doi.org/10.1016/j.powtec.2021.08.059

Ghafori, H., & Sharifi, M. (2018). Numerical and experimental study of an innovative design of elbow in the pipe line of a pneumatic conveying system. *Powder Technology*, *331*, 171–178. https://doi.org/10.1016/j.powtec.2018.03.022

Gimbun, J., Chuah, T. G., Fakhru, A., & Choong, T. S. Y. (2005). The influence of temperature and inlet velocity on cyclone pressure drop : A CFD study. Chemical Engineering and Processing: *Process Intensification*, *44*(1), 7–12. https://doi.org/10.1016/j.cep.2004.03.005

Gonite, T. (2018). Design and prototyping of teff (ጤፍ) row planter and fertilizer applier. *International Journal of Mechanical Engineering and Applications*, *6*(4), 91. https://doi.org/10.11648/j.ijmea.20180604.11

Huang, F., Zhu, Q., Zhou, X., Gou, D., Yu, J., Li, R., Tong, Z., & Yang, R. (2021). Role of CFD based in silico modelling in establishing an in vitro-in vivo correlation of aerosol deposition in the respiratory tract. *Advanced Drug Delivery Reviews*, *170*, 369-385. https://doi.org/10.1016/j.addr.2020.09.007

Kaya, F., & Karagoz, I. (2012). Experimental and numerical investigation of pressure drop coefficient and static pressure difference in a tangential inlet cyclone separator. *Chemical Papers*, *66*(11), 1019–1025. https://doi.org/10.2478/s11696-012-0214-7

Khazaee, I. (2017). Numerical investigation of the effect of number and shape of inlet of cyclone and particle size on particle separation. *Heat and Mass Transfer/Waerme- Und Stoffuebertragung*, *53*(6), 2009–2016. https://doi.org/10.1007/s00231-016-1957-4

Ma, A. C., Williams, K. C., Zhou, J. M., & Jones, M. G. (2010). Numerical study on pressure prediction and its main influence factors in pneumatic conveyors. *Chemical Engineering Science*, *65*(23), 6247–6258. https://doi.org/10.1016/j.ces.2010.09.010

Ripp, M., Debele, Z. A., & Ripperger, S. (2015). Determination of bulk flow property of tef flour and seed and design of a silo. *Particulate Science and Technology*, *33*(5), 494–502. https://doi.org/10.1080/02726351.2014.1003626

Roberts, J., Wypych, P., Hastie, D., & Liao, R. (2022). Analysis and validation of a CFD-DPM method for simulating dust suppression sprays. *Particulate Science and Technology*, *40*(4), 415–426. https://doi.org/10.1080/02726351.2021.1951907

Safikhani, H., Esmaeili, F., & Salehfard, S. (2020). Numerical study of flow field in new design dynamic cyclone separators. *International Journal of Engineering, Transactions B: Applications*, *33*(2), 357–365. https://doi.org/10.5829/IJE.2020.33.02B.22

Singh, J., Gill, H. S., & Vasudev, H. (2023). Computational fluid dynamics analysis on role of particulate shape and size in erosion of pipe bends. *International Journal on Interactive Design and Manufacturing*, *17*(5), 2631–2646.

https://doi.org/10.1007/s12008-022-01094-7

Sommerfeld, M. (2003). Analysis of collision effects for turbulent gas-particle flow in a horizontal channel: Part I. Particle transport. *International Journal of Multiphase Flow*, *29*(4), 675–699. https://doi.org/10.1016/S0301-9322(03)00031-4

intralogistic bulk material handling processes using fuzzy step-wise weight assessment ratio analysis and axial-distance-based aggregated measurement methods. *Applied Sciences (Switzerland)*, *14*(4). https://doi.org/10.3390/app14041549

Vandercasteelen, J., Dereje, M., Minten, B., & Taffesse, A. S. (2014). Perceptions, impacts and rewards of row planting of teff. *SSRN Electronic Journal*, *May*. https://doi.org/10.2139/ssrn.2530422

Wang, C., Li, W., Li, B., Jia, Z., Jiao, S., & Ma, H. (2023). Study on the influence of different factors on pneumatic conveying in horizontal pipe. *Applied Sciences (Switzerland)*, *13*(9). https://doi.org/10.3390/app13095483

Wu, X., Liu, J., Xu, X., & Xiao, Y. (2011). Modeling and experimental validation on pressure drop in a reverse-flow cyclone separator at high inlet solid loading. *Journal of Thermal Science*, *20*(4), 343–348. https://doi.org/10.1007/s11630-011-0479-0

Tadele, E., & Hibistu, T. (2021). Empirical review on the use dynamics and economics of teff in Ethiopia. *Agriculture & Food Security*, *10*, 1-13. https://doi.org/10.1186/s40066-021-00329-2

Tadić, S., Krstić, M., Božić, M., Dabić-Miletić, S., & Zečević, S. (2024). Ranking of technologies for

Xu, Z., Fei, Z., Zhu, Y., Wang, C., Yang, X., Guo, L., Xue, G., & Liu, Y. (2024). The numerical investigation of solid–liquid two-phase flow characteristics inside and outside a newly designed 3d sediment trap. *Journal of Marine Science and Engineering*, *12*(1). https://doi.org/10.3390/jmse12010016

Zewdu, A. D. (2007). Aerodynamic properties of tef grain and straw material. *Biosystems Engineering*, *98*(3), 304–309. https://doi.org/10.1016/j.biosystemseng.2007.08.003

Zhao, B. (2009). Modeling pressure drop coefficient for cyclone separators: A support vector machine approach. *Chemical Engineering Science*, *64*(19), 4131–4136. https://doi.org/10.1016/j.ces.2009.06.017